Mid-infrared-to-mid-ultraviolet supercontinuum enhanced by third-to-fifteenth odd harmonics

A. V. Mitrofanov,[1,2,3,4] A. A. Voronin,[1,2] S. I. Mitryukovskiy,[1] D. A. Sidorov-Biryukov,[1,2] A. Pugžlys,[5,6] G. Andriukaitis,[5] T. Flöry,[5] E. A. Stepanov,[1,2] A. B. Fedotov,[1,2] A. Baltuška,[5,6] and A. M. Zheltikov[1,2,3,7,*]

[1]*Russian Quantum Center, ul. Novaya 100, Skolkovo, Moscow Region 143025, Russia*

[2]*Physics Department, International Laser Center, M.V. Lomonosov Moscow State University, Moscow 119992, Russia*

[3]*Kurchatov Institute National Research Center, Moscow 123182, Russia*

[4]*Institute of Laser and Information Technologies, Russian Academy of Sciences, Shatura, Moscow Region 140700, Russia*

[5]*Photonics Institute, Vienna University of Technology, Gusshausstrasse 27-387, 1040 Vienna, Austria*

[6]*Center for Physical Sciences & Technology, Savanoriu Ave. 231, LT-02300 Vilnius, Lithuania*

[7]*Department of Physics and Astronomy, Texas A&M University, College Station, Texas 77843, USA*

**Corresponding author: zheltikov@physics.msu.ru*

Received January 26, 2015; revised March 22, 2015; accepted March 26, 2015;
posted March 31, 2015 (Doc. ID 232712); published April 29, 2015

A high-energy supercontinuum spanning 4.7 octaves, from 250 to 6500 nm, is generated using a 0.3-TW, 3.9-μm output of a mid-infrared optical parametric chirped-pulse amplifier as a driver inducing a laser filament in the air. The high-frequency wing of the supercontinuum spectrum is enhanced by odd-order optical harmonics of the mid-infrared driver. Optical harmonics up to the 15th order are observed in supercontinuum spectra as overlapping, yet well-resolved peaks broadened, as verified by numerical modeling, due to spatially nonuniform ionization-induced blue shift.

OCIS codes: (190.7110) Ultrafast nonlinear optics; (190.5940) Self-action effects.
http://dx.doi.org/10.1364/OL.40.002068

Broadband sources of coherent radiation in the mid-infrared (mid-IR) range are in great demand for a broad variety of applications, including molecular vibrational spectroscopy [1], semiconductor optoelectronics [2], frequency-comb technologies [3], trace-gas detection [4], biomedical diagnostics [5], and food quality control [6]. Due to their unsurpassed brightness, synchrotron-based mid-IR beamlines enable a high-resolution chemically sensitive imaging with fast image acquisition and high signal-to-noise ratio within the entire mid-IR range [7,8]. As a way toward lower costs and real-life-friendly formats, nonlinear-optical methods of mid-IR supercontinuum generation have been demonstrated using properly chosen solid-state materials [9,10] and nonsilica fibers [11]. The energy and the peak power of these mid-IR supercontinuum sources are, however, limited as the intensity of the driver needs to be kept below the laser damage threshold in the bulk of a solid or in a fiber.

Supercontinua with peak powers well above the limits dictated by laser damage thresholds of solid materials can be generated by high-power ultrashort light pulses inducing laser filaments in gas media [12,13]. In the mid-IR range, filamentation in the gas phase has become possible only recently [14,15], since the development of high-peak-power mid-infrared optical parametric chirped-pulse amplifiers (OPCPAs) [16]. In the first gas-phase filamentation experiments in the mid-infrared, performed with 0.1-TW mid-infrared pulses focused in high-pressure gases [14], spectral broadening of the mid-infrared driver was accompanied by efficient energy conversion to the third and fifth harmonics of the driver. In this work, much more powerful, 0.25-TW mid-IR pulses with a sub-100-fs pulse width at a central wavelength of 3.9 μm are used to induce a laser filament in the air. At this level of peak powers, odd harmonics up to the 15th order, broadened due to spatially nonuniform ionization-induced blue shift, are shown to prominently contribute to supercontinuum generation. Notably, when Ti: sapphire laser pulses are used to induce filaments in the atmospheric air, generation of optical harmonics beyond the third order is not possible because of the absorption of the atmosphere. For the mid-IR driver used in experiments presented in this work, harmonics up to the 15th order fall within the transmission range of the atmospheric air. Moreover, as shown earlier for the third to seventh odd harmonics of a mid-IR driver [17], the weakness of dispersion of the atmospheric air in the mid-infrared favors phase matching for the generation of these harmonics. In experiments presented below in this report, we show that optical harmonics can radically enhance the high-frequency part of the supercontinuum generated by a high-peak-power mid-IR driver, yielding a high-energy broadband radiation with a spectrum spanning over four octaves, from 250 to at least 6500 nm.

High-power ultrashort mid-IR driver pulses are delivered in our experiments by the Skolkovo version of a high-power OPCPA source [15], consisting of a solid-state ytterbium laser with an amplifier, a three-stage optical parametric amplifier (OPA), a grism stretcher, a Nd: YAG pump laser, a three-stage OPCPA system, and a grating compressor for mid-IR pulses. The 1-kHz, 200-fs, 1–2-mJ, 1030-nm regeneratively amplified output of the Yb:CaF_2 laser system is used as a pump for the three-stage OPA, which generates 200-fs 1460-nm pulses at its output. These 1460-nm pulses are then stretched with a grism stretcher and used as a seed in a three-stage OPCPA, consisting of three KTA crystals I, II, and III, pumped by 100-ps Nd: YAG-laser pulses with energies 50, 250, and 700 mJ, respectively. The stretched-pulse idler-wave output of the OPCPA system has a central

wavelength of 3.9 μm and an energy above 50 mJ. Compression of these pulses using a grating compressor yields 90-fs mid-IR pulses with an energy up to 30 mJ.

Spectral measurements in the mid-IR range are performed with a homebuilt scanning monochromator and a thermoelectrically cooled HgCdTe detector. For the spectral measurements in the ultraviolet, visible, and near-IR ranges, OceanOptics HR4000 and NIRQuest spectrometers were employed. Temporal envelopes and phases of mid-infrared pulses are characterized using frequency-resolved optical gating (FROG) based on second-harmonic generation (SHG) in a 0.5-mm-thick $AgGaS_2$ crystal. A typical SHG FROG trace of the compressed mid-IR OPCPA output is shown in Fig. 1(a). The pulse envelope and phase retrieved from this FROG trace is presented in Fig. 1(b). The spectrum retrieved from the SHG FROG trace [dashed line in Fig. 1(c)] agrees well with the spectrum measured by the scanning monochromator and the HgCdTe detector [solid line in Fig. 1(c)]. The beam profile of the mid-IR OPCPA output is shown in Fig. 1(d).

A 3.9-μm, 25-mJ, 90-fs driver used in our experiments has a peak power $P \approx 280$ GW, which is a factor of 3.5 higher than the critical power of self-focusing of 3.9-μm radiation in the atmospheric air, $P_{cr} \approx 80$ GW. When focused by a parabolic mirror with a focal length of 0.5 m, such driver pulses induce a filament with a total length of about 10 cm. Laser filamentation in the atmosphere is accompanied by a generation of broadband, white-light radiation. With an appropriate focusing of the driver, the spectrum of this radiation continuously spans a wavelength range of at least 4.7 octaves, stretching from 250 to 6500 nm (Fig. 2). For longer wavelengths, the sensitivity of the mid-IR spectrometer rapidly falls off, making spectral measurements unreliable. The high-frequency part of the supercontinuum is drastically enhanced by odd-order harmonics of the driver. Odd harmonics up to the 15th order are clearly seen in supercontinuum spectra in Fig. 2 as spectrally broadened, still well-resolved peaks near the frequencies $(2m+1)\omega_0$, where m is an integer and ω_0 is the central frequency of the mid-infrared driver.

With the parameters of the mid-IR driver fixed, the efficiency of driver energy conversion to the harmonics is controlled by the focal length f of the mirror used to focus the pump beam. The maximum efficiency of energy conversion into the spectrally broadened third harmonic, defined as the energy emitted in the 980–1960-nm range of the supercontinuum spectrum to the total input energy of the driver, is achieved with $f = 50$ cm, and is estimated as $\eta_3 \approx 0.1\%$ with 10% energy fluctuation. The $f = 50$ cm mirror also maximizes the total efficiency of energy conversion to all the harmonics, from the third to the fifteenth, $\eta_\Sigma \approx 0.13\%$.

Analysis of the supercontinuum beam profile reveals a complex, nonuniform distribution of spectral components over the supercontinuum beam (the inset in Fig. 2). As one of the most striking tendencies, the off-axial spectra display a strong blue shift relative to their on-axis counterparts. As a result, the off-axial harmonic signals are also systematically blue-shifted relative to the on-axis harmonic spectra. An almost perfect axial symmetry of the beam behind the filament (the inset in Fig. 2) indicates that only one filament is formed in the atmosphere in our experiments. This result is predictable for a driver with a peak power $P \approx 3.5P_{cr}$, used in our experiments, and is verified by numerical simulations.

To analyze the spatiotemporal field dynamics behind filamentation-assisted supercontinuum generation, we use a model based on the field evolution equation [12,13,17] that includes the dispersion of the medium, beam diffraction, neutral-gas and ionization-induced optical nonlinearities, pulse self-steepening, spatial self-action phenomena, as well as plasma-related loss, refraction, and dispersion. Optical harmonic generation is included in this analysis perturbatively, through the relevant nonlinear susceptibilities. The field evolution equation is solved jointly with the equation for the electron density with the photoionization rate calculated using the Popov–Perelomov–Terentyev version of the Keldysh formalism [12,13]. Simulations were performed

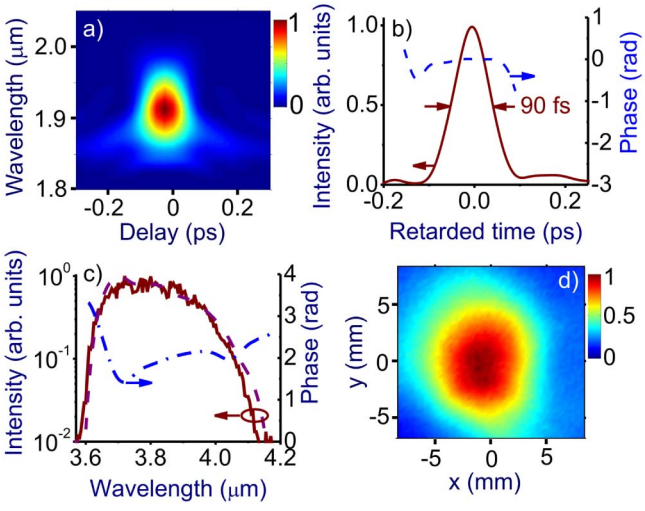

Fig. 1. (a) Typical SHG FROG trace of the compressed mid-IR OPCPA, (b) the pulse envelope (solid line) and phase (dashed line) retrieved from this FROG trace, (c) the spectrum (dashed line) and spectral phase (dashed–dotted line) retrieved from the SHG FROG trace and the spectrum measured with the scanning monochromator and the HgCdTe detector (solid line), and (d) the beam profile of the mid-IR OPCPA output.

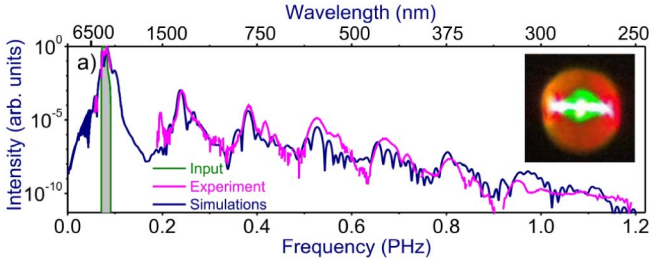

Fig. 2. On-axis spectrum of supercontinuum radiation generated in a filament induced by the mid-IR OPCPA output in the air: (red) experiment, (blue) simulations. The spectrum of the mid-IR driver inducing the filament is shown with grey shading. The supercontinuum beam behind the filament is shown in the inset.

using an MPI parallel programming interface on the Chebyshev and Lomonosov supercomputer clusters of Moscow State University for driver pulses used in experiments, i.e., a central wavelength of 3.9 μm, pulse width of 90 fs, an energy of 25 mJ, and a beam diameter of 1.5 cm.

With a standard set of constants for the dispersion, nonlinearity, and ionization for the atmospheric air, numerical simulations accurately reproduce the experimental spectra (Fig. 2) and the energies of harmonic signals, offering important insights into the physics behind supercontinuum generation in the filament. While reliable spectral measurements for wavelengths longer than 6.5 μm were not possible in our experiments, simulations, as can be seen from Fig. 2(a), suggest that the mid-IR wing of the supercontinuum spectrum continuously extends well beyond 6.5 μm, yielding an overall supercontinuum bandwidth well above five octaves.

Typical spatiotemporal dynamics of a mid-IR driver inducing a filament in our experimental conditions is illustrated in Figs. 3(a)–3(d). As long as the field intensity is low in the leading edge of the pulse [$\tau = -50$ fs in Fig. 3(a), where τ is the time in the frame of reference running with the group velocity of the driver pulse, with $\tau = 0$ corresponding to the center of the input pulse], self-focusing and ionization effects are negligible. The beam dynamics in this section of the pulse is dominated by diffraction. However, as the field intensity increases toward the central part of the pulse, nonlinear phenomena and gas ionization become significant [Fig. 3(b)]. The central part of the mid-infrared driver and its trailing edge propagate in a medium where a transient electron-density gradient has been induced by the leading edge of the pulse, undergoing a scattering off this electron-density gradient [Figs. 3(c) and 3(d)]. Strong interaction of this part of the beam with the plasma that the leading edge of the pulse leaves behind induces a dramatic blue shift, observed as an intense off-axial feature stretching from the central wavelength of the driver in the mid-IR up to 1.5 μm in Fig. 3(e). As a part of subsequent filamentation dynamics, this scattered beam fraction is refocused due to self-focusing [Figs. 3(c) and 3(d)], forming a filament in the central part of the beam. Much longer filaments could be induced by driver pulses with smaller beam diameters focused by longer focal-length mirrors. In particular, filaments whose lengths exceeded 1 m were generated by using 7-mm-diameter mid-IR driver beam focused with a 2-m-focal-length mirror. However, the spectra of supercontinua generated in such long filaments are not as broad as the supercontinuum spectrum shown in Fig. 2.

Filamentation of the mid-IR driver in the air is accompanied by efficient odd-order harmonic generation. At $z = 45$ cm, optical harmonics show up [Fig. 4(a)] as well-resolved equidistant signals in the spectrum of the field centered at $(2m + 1)\omega_0$. At this stage, both the pulse width and the beam diameter of each harmonic decrease with the harmonic order due to the increasing order of nonlinearity. With $z > 46$ cm, effects related to ionization-induced defocusing become noticeable, decreasing the field intensity on the trailing edge of the pulse [Figs. 3(a)–3(d)]. This effect suppresses harmonic generation in the trailing edge of the pulse, confining this process to the leading edge and the central part of the pulse, where ionization-induced defocusing is less dramatic.

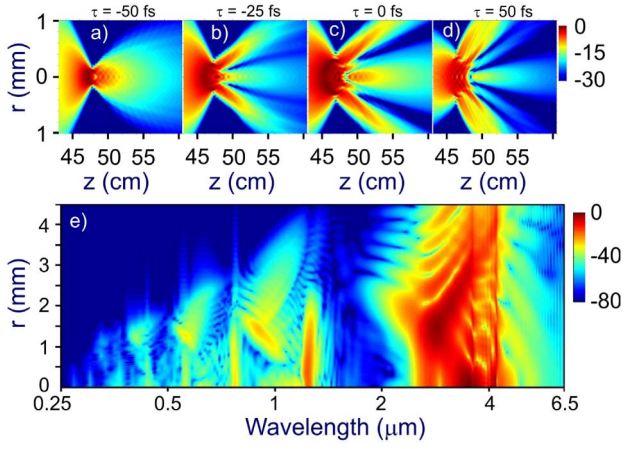

Fig. 3. (a)–(d) Time-resolved beam dynamics calculated for different sections of the mid-infrared driver pulse at the distance from the focusing mirror $z = 62$ cm, with (a) $\tau = -50$ fs, (b) −25 fs, (c) 0 fs, and (d) 50 fs. (e) Radially resolved spectra of the supercontinuum generated in a filament induced by the mid-IR OPCPA output in the air.

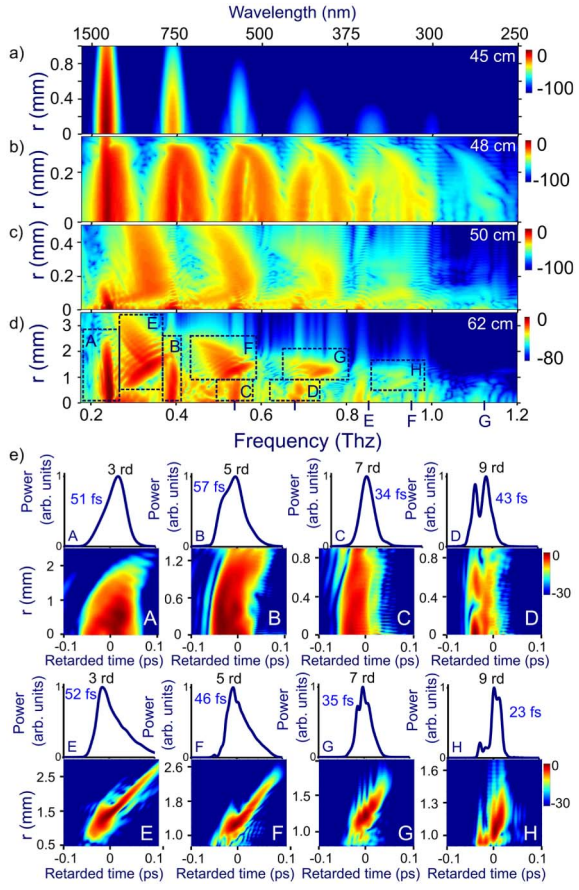

Fig. 4. (a)–(d) Radially resolved spectra of optical harmonics in a filament induced by the mid-IR OPCPA output in the air at $z = 45$ cm (a), 48 cm (b), 50 cm (c), and 62 cm (d). (e) Pulse envelopes and spatiotemporal maps of on-axis (boxes A–D) and off-axis (boxes E–H) optical harmonics at $z = 62$ cm isolated from the overall harmonic field as shown in panel (d).

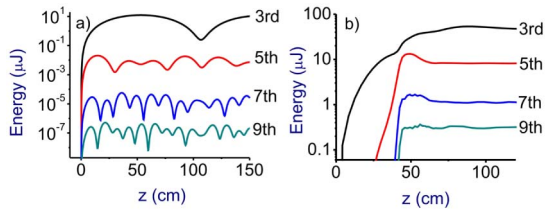

Fig. 5. The total energy in the third (black), fifth (red), seventh (blue), and ninth (green) optical harmonic calculated as a function of the propagation length in a collimated-beam geometry (a) and in a laser-induced filament (b) for a 0.25-TW, 80-fs, 3.9-μm pump pulse.

Further on along the beam path, with $z > 47$ cm, the off-axial beam fraction, arising in the trailing edge of the pulse [Figs. 3(c) and 3(d)], starts serving as a source for off-axial harmonic generation [Figs. 4(b) and 4(c)]. Since the outer sections of the beam are formed due to a strong scattering of radiation off the electron density profile [Figs. 3(c) and 3(d)], these parts of the beam, as can be seen in Figs. 4(b) and 4(c), exhibit a much stronger blue shift. As a result, the off-axis optical harmonics are also blue-shifted relative to the harmonics generated along the beam axis. For $z > 50$ cm, beam refocusing on the trailing edge of the pulse becomes noticeable [Figs. 3(c) and 3(d)], giving rise to additional peaks in the temporal profiles of optical harmonics toward the back of the driver pulse [boxes G and H in Fig. 4(e)]. Simulations presented in Figs. 4(b)–4(d) show how this blue shift of the off-axial harmonics builds up, increasing toward the output end of the filament [see also Fig. 3(e)], reproducing the main features of the supercontinuum spectra measured in experiments at $z \approx 62$ cm.

In Figs. 5(a) and 5(b), we compare odd-order harmonic generation in a laser filament with the buildup of optical harmonics in the collimated-beam regime [18]. In the collimated-beam geometry, harmonic intensities calculated as functions of the propagation length z exhibit characteristic well-resolved fringes [Fig. 5(a)], controlled by the coherence lengths for the relevant direct and cascaded harmonic-generation processes. As can be seen from Fig. 5(b), in the filamentation regime, the coherence length of third-harmonic generation in the atmospheric air ($l_{\mathrm{th}} \approx 50$ cm) is still a meaningful physical scale. As long as $z \ll l_{\mathrm{th}}$, the third harmonic grows approximately as z^2, reaching saturation when z approaches l_{th}. Since the third harmonic strongly contributes to the generation of higher order harmonics through cascaded wave mixing, the higher order harmonics are seen to rapidly build up within a short distance near $z \approx l_{\mathrm{th}}$. Remarkably, despite the complexity of beam dynamics in a laser filament, with appropriate optimization, achieved for our experimental conditions with $f \approx 50$ cm, the efficiencies of harmonic generation in a laser filament can be almost an order of magnitude higher than the efficiencies attainable in the collimated-beam geometry [cf. Figs. 5(a) and 5(b)]. This becomes possible due to the additional channel of energy transfer from the pump to optical harmonics provided by off-axial harmonic generation [Figs. 4 and 5].

To summarize, laser filaments induced in the air by 0.25-TW, sub-100-fs pulses with a central wavelength of 3.9 μm are shown to enable the generation of high-energy supercontinuum spanning at least 4.7 octaves, from 250 to 6500 nm. Optical harmonics up to the 15th order are produced in such laser filaments, providing energy conversion to the third harmonic up to 0.1%.

This research was supported in part by the Russian Foundation for Basic Research (Project Nos. 13-02-01465, 14-29-07182, 14-02-00784, and 14-22-02099) and the Welch Foundation (Grant No. A-1801). Research into the nonlinear optics in the mid-infrared has been supported by the Russian Science Foundation (Project No. 14-12-00772).

References

1. J. M. Chalmers and P. R. Griffiths, eds., *Handbook of Vibrational Spectroscopy* (Wiley, 2002).
2. A. Krier, ed., *Mid-infrared Semiconductor Optoelectronics* (Springer, 2006), Vol. **118**.
3. A. Schliesser, N. Picqué, and T. W. Hänsch, Nat. Photonics **6**, 440 (2012).
4. M. Jahjah, W. Jiang, N. P. Sanchez, W. Ren, P. Patimisco, V. Spagnolo, S. C. Herndon, R. J. Griffin, and F. K. Tittel, Opt. Lett. **39**, 957 (2014).
5. S. Liakat, K. A. Bors, L. Xu, C. M. Woods, J. Doyle, and C. F. Gmachl, Biomed. Opt. Express **5**, 2397 (2014).
6. J. Wegener, R. H. Wilson, and H. S. Tapp, Trends Anal. Chem. **18**, 14 (1999).
7. M. J. Nasse, M. J. Walsh, E. C. Mattson, R. Reininger, A. Kajdacsy-Balla, V. Macias, R. Bhargava, and C. J. Hirschmugl, Nat. Methods **8**, 413 (2011).
8. M. C. Martin, C. Dabat-Blondeau, M. Unger, J. Sedlmair, D. Y. Parkinson, H. A. Bechtel, B. Illman, J. M. Castro, M. Keiluweit, D. Buschke, B. Ogle, M. J. Nasse, and C. J. Hirschmugl, Nat. Methods **10**, 861 (2013).
9. F. Silva, D. R. Austin, A. Thai, M. Baudisch, M. Hemmer, D. Faccio, A. Couairon, and J. Biegert, Nat. Commun. **3**, 807 (2012).
10. A. A. Lanin, A. A. Voronin, E. A. Stepanov, A. B. Fedotov, and A. M. Zheltikov, Opt. Lett. **40**, 974 (2015).
11. C. R. Petersen, U. Møller, I. Kubat, B. Zhou, S. Dupont, J. Ramsay, T. Benson, S. Sujecki, N. Abdel-Moneim, Z. Tang, D. Furniss, A. Seddon, and O. Bang, Nat. Photonics **8**, 830 (2014).
12. A. Couairon and A. Mysyrowicz, Phys. Rep. **441**, 47 (2007).
13. L. Berge, S. Skupin, R. Nuter, J. Kasparian, and J.-P. Wolf, Rep. Prog. Phys. **70**, 1633 (2007).
14. D. Kartashov, S. Ališauskas, A. Pugžlys, A. Voronin, A. Zheltikov, M. Petrarca, P. Béjot, J. Kasparian, J.-P. Wolf, and A. Baltuška, Opt. Lett. **38**, 3194 (2013).
15. A. V. Mitrofanov, A. A. Voronin, D. A. Sidorov-Biryukov, A. Pugžlys, E. A. Stepanov, G. Andriukaitis, T. Flöry, S. Ališauskas, A. B. Fedotov, A. Baltuška, and A. M. Zheltikov, Sci. Rep. **5**, 8368 (2015).
16. G. Andriukaitis, T. Balčiūnas, S. Ališauskas, A. Pugžlys, A. Baltuška, T. Popmintchev, M.-C. Chen, M. M. Murnane, and H. C. Kapteyn, Opt. Lett. **36**, 2755 (2011).
17. D. Kartashov, S. Ališauskas, A. Pugžlys, A. A. Voronin, A. M. Zheltikov, and A. Baltuška, Opt. Lett. **37**, 2268 (2012).
18. Y. R. Shen, *The Principles of Nonlinear Optics* (Wiley-Interscience, 1984).